Polymer 50 (2009) 4671–4682

Contents lists available at ScienceDirect

Polymer

journal homepage: www.elsevier.com/locate/polymer

Novel polypropylene microporous membranes via spherulitic deformation – Processing perspectives

K.-Y. Lin, M. Xanthos*, K.K. Sirkar**

Otto York Department of Chemical, Biological and Pharmaceutical Engineering, Center for Membrane Technologies, New Jersey Institute of Technology, Newark, NJ 07102, United States

ARTICLE INFO

Article history:
Received 30 March 2009
Received in revised form
29 June 2009
Accepted 4 July 2009
Available online 15 July 2009

Keywords:
Melt processing
Spherulite
Polypropylene

ABSTRACT

The processing boundaries for initiating intra-/inter-spherulitic deformation to create microporous polypropylene membranes by lamellar separation are delineated. The processing parameters are: annealing temperature, extension ratio, stretching rate, and stretching temperature. A fixed set of extrusion conditions was chosen for producing precursor films having similar spherulitic morphologies. The morphological changes indicating the occurrence of intra-/inter-spherulitic transition on a spherulitic scale can also be detected on a lamellar scale by WAXS examination via analysis of the α-form orientation index. Membrane porosity measurements showed a consistent correlation with the observed values of the α-form orientation index. Increasing the extension ratio did not change the microstructure in the non-annealed sample; however, the lamellae can be further oriented in the annealed samples. Inter-spherulitic deformation became obvious at slow stretching rates; intra-spherulitic deformation was favored at fast stretching rates. The DSC thermal analysis of the precursor films showed two significant endothermic discontinuities (T_1 at 0 °C and T_2 at 40 °C) in both non-annealed and annealed precursor films; T_1 is believed to be the conventional T_g of polypropylene whereas T_2 appears to originate from the rigid-amorphous fraction trapped within the lamellar "wells" where the amorphous phase is surrounded by the R-lamellae and the T-lamellae. The lamellae could break down or slip from the lamellar knots as stretching temperatures are high enough to minimize the influence of the rigid-amorphous fraction, and the annealed lamellae can still be oriented without a catastrophic cold-drawn deformation.

1. Introduction

Semicrystalline polymers, such as polyethylene and polypropylene, are important commodity plastics due to their low cost and robust properties. Their good mechanical properties as well as good solvent resistance are due to the presence of a crystalline phase which resides in the crystalline/amorphous matrix. These semicrystalline polymers are excellent candidates for making solvent-resistant microporous separation membranes. The difficulty in dissolving of the crystalline phase has limited their applicability to the conventional membrane solvent casting process also known as non-solvent induced phase separation (NIPS) process, where the porous structure of the membranes is created by the phase separation induced by the addition of a non-solvent to the polymer solution. Another widely used method to create porous membranes with semicrystalline polymers is to utilize temperature gradients in a polymer paste (polymer with lubricant) to initiate the phase separation. This is also known as the thermally induced phase separation (TIPS) process [1]. The required lubricant extraction process and larger pore sizes are drawbacks of this technique.

An alternative method for creating porous structures in semicrystalline polyolefins has been established successfully since the 1970s under the trade name "Celgard®" [2,3]. In this process, the porous structure is generated by the deformation of aligned crystalline domains (row lamellae) which is created at high-stress extrusion conditions. Semicrystalline polymers cannot fully crystallize as a result of their high molecular weight and broad molecular weight distribution, even if they possess a highly stereo-regular configuration. The crystalline phase is composed of a chain folding lamellar morphology sandwiched by amorphous regions [4]. When crystallization occurs under a no-stress environment, the lamellae grow radially from nucleated sites and form a spherulite. The spherulites keep growing until they impinge onto each other. The lamellae can also form a shish–kebab structure or a stacked row lamellar structure under a high-stress environment, which is an important step for the Celgard® membrane. The slit-like, sub-micron pores with narrow pore size distribution are generated by separating row lamellae in

* Corresponding author. Tel.: +1 973 642 4762; fax: +1 973 596 8436.
** Corresponding author. Tel.: +1 973 596 8447; fax: +1 973 642 4854.
E-mail addresses: xanthos@njit.edu (M. Xanthos), sirkar@njit.edu (K.K. Sirkar).

0032-3861/$ – see front matter © 2009 Elsevier Ltd. All rights reserved.
doi:10.1016/j.polymer.2009.07.014

a subsequent stretching step. A distinct "hard-elastic" mechanical response due to the nature of stacked lamellae is exhibited during the stretching step [2], which also gives the membrane excellent mechanical strength along the machine direction. However, the low mechanical strength in the transverse direction results in splitting problems during assembling of the membrane in various devices [5].

A different strategy employing the deformation of the spherulitic structure has been investigated in our recent work [6]. Even though the formation and deformation mechanisms of the spherulitic structure have been studied for a long time [7–10], such concepts have not been applied to the fabrication of porous structures. This might be due to the morphological complexity of spherulites, such as their size and size distribution [9], and an even more complicated behavior as they deform [7,11]. The idea of using spherulitic deformation to create porous structures becomes possible by utilizing the strengthened spherulitic structure in the α-form of isotactic polypropylene. It is known that α-PP has a cross-hatched lamellar morphology unique among semicrystalline polymers [11]. The lamellar growing directions of α-PP can be radial and tangential depending on the cooling rate [12]. Due to a small mismatch in the *a*-axis and *c*-axis of its monoclinic unit cell, the tangential lamellae (T-lamellae) are formed on top of the *a*–*c* plane of the radial lamellae (R-lamellae) with a branching angle of 80° [13]. There are two important features of this unique lamellar morphology for creating porous structures in a spherulitic film. First, the presence of T-lamellae improves the strength of spherulites by acting like "knots", which provide anchor spots when the spherulites deform. Aiding by this interlocking morphology, α-PP spherulites are more rigid and appear capable of maintaining their spherulitic morphology upon loading [8,14]. Secondly, the T-lamellae can act as extra space restraints during lamellar opening and this may lead to smaller pores.

The separation of lamellae of semicrystalline polymers with spherulitic features can occur intra-spherulitically or inter-spherulitically [7,15]. Intra-spherulitic deformation shows necking and cold-drawing appearance when the sample is stretched beyond its yield point [10]. Catastrophic lamellar breaking and chain orientation occurs inside the spherulites. Then, a highly oriented and tightly packed lamellar structure is formed until the final structure breaks down. On the other hand, inter-spherulitic deformation often shows a fracture surface along the spherulitic boundary when the lamellae inside the spherulites are better organized under slow crystallization conditions. In fact, the separated spherulitic boundary in inter-spherulitic deformation is filled up with residual lamellae before fracture occurs. A potentially well-connected porous region may be created along the separated spherulitic boundary. Furthermore, the occurrence of inter-spherulitic deformation could relieve the stress which leads to catastrophic lamellar separation initiated by intra-spherulitic deformation.

The combination of intra-/inter-spherulitic deformations to create microporous membranes by lamellar separation has been presented in our previous work [6]. A precursor film with spherulitic features is extruded, and the porous structure is created in a following stretching step. The processing conditions employed to demonstrate the validity of the concept are addressed in this study. The investigated parameters include: (1) annealing temperature of precursor films; (2) extension ratio, stretching rate, and stretching temperature of the stretched membranes.

2. Experimental

2.1. Materials

A film extrusion grade PP, Dow H314-02Z, was used. It is a homopolymer with density of 0.9 g/cm^3 and MFR (melt flow rate) of 2 g/10 min.

2.2. Membrane fabrication

2.2.1. Step I: Precursor film extrusion

The precursor films were extruded through a Brabender single screw extruder ($D = 1.8$ cm, $L/D = 15$) equipped with a 15 cm sheet die. The extrusion conditions were selected to ensure the formation of spherulitic structures instead of stacked row lamellar structures in the precursor films. The temperature setting of the extruder was 230 °C; the extrusion speed was 30 rpm. The die-lip gap was fixed at 100 μm. A three-layer take-up roll was used to collect the extruded film. The roll temperature was maintained at 90 °C by a circulating water bath. The distance between the extrusion die and the collecting roll was kept at 2.5 cm. The take-up speed was kept low to avoid generating additional orientation in the precursor films. The thickness of the precursor films was about 70 μm.

2.2.2. Step II: Annealing

The precursor films were annealed in an air-circulating oven for 2 h. A long annealing time was selected to ensure that a steady temperature was reached. The annealing temperatures were set at 100 °C, 120 °C, and 140 °C. The appearance and thermal analysis results of the annealed samples showed no sign of degradation. Samples designated as (An 100C), (An 120C), etc. were annealed at 100 °C, 120 °C, etc.

2.2.3. Step III: Uniaxial stretching

A Tinius Olsen LOCAP universal testing machine equipped with a temperature control chamber was used for the stretching step. The non-annealed and annealed precursor films were cut as 7.6 cm wide rectangular sheets before stretching. The stretching direction was parallel to the extrusion direction, which is designated as the machine direction. The films were held between two air-pressurized clamps with an initial distance between the clamps being 2.5 cm. The stretching rates (R_S) ranged from 0.25 cm/min to 50.8 cm/min. The extension ratios (E_S) of the films ranged from 100% (from the original length) to 600%. The stretching temperatures (T_S) were −20 °C, 25 °C, and 70 °C. Most of the samples were stretched at $R_S = 12.7$ cm/min, $E_S = 200\%$, and $T_S = 25$ °C. The stretched membranes were then held under tension at 90 °C for 10 min followed by cooling down to 25 °C for 20 min to stabilize the structure. The final membrane thickness varied from 10 to 35 μm.

2.3. Characterization

2.3.1. Wide angle X-ray scattering (WAXS)

The wide angle X-ray scattering pattern of the films was recorded by a Philips PW3040 X-ray Diffractometer with a Cu Kα radiation ($\lambda = 1.54$ Å) and a 2θ range from 10° to 24°.

2.3.2. Polarizing optical microscopy (POM)

Precursor films were analyzed using a Zeiss polarizing optical microscope, and the image was collected by a Zeiss image adapter and recorded on the computer.

2.3.3. Scanning electron microscopy (SEM)

The SEM images were obtained by a Leo 1530 VP field emission scanning electron microscope (FESEM). In order to prevent charge accumulation on the sample surface during examination, all samples were pre-coated with a thin layer of gold/platinum alloy. The effect of coating conditions, such as sputtering time, applied current for sputtering and distance between sample stage and sputter, was carefully checked to prevent artifacts, especially under high magnification. The voltage applied during SEM observation was low (1–3 kV); the effect of surface rupture due to applied energy was not evident during SEM observation.

2.3.4. Differential scanning calorimetry (DSC)

DSC tests of the precursor films were carried out on a TA instrument Q100 with sample weight of about 5 mg. For melting temperature measurements, the heating rate was 10 °C/min and the scan range was from −50 °C to 200 °C. For crystallization temperature measurements, the samples were first kept isothermally at 200 °C for 5 min to erase their thermal history and then cooled down to 25 °C at 10 °C/min. The crystallinity of the sample was calculated from enthalpy change values obtained in the heating curve, and by assuming 209 J/g as the heat of fusion of a 100% crystalline sample [11].

2.3.5. Porosity measurements

The porosity (ε) of the stretched membranes was calculated from the following equations:

$$\rho_{cal} = \rho_c \chi_c + \rho_a (1 - \chi_c) \quad (1)$$

$$V_{cal} = M_M / \rho_{cal} \quad (2)$$

$$\varepsilon = \frac{V_M - V_{cal}}{V_{cal}} \quad (3)$$

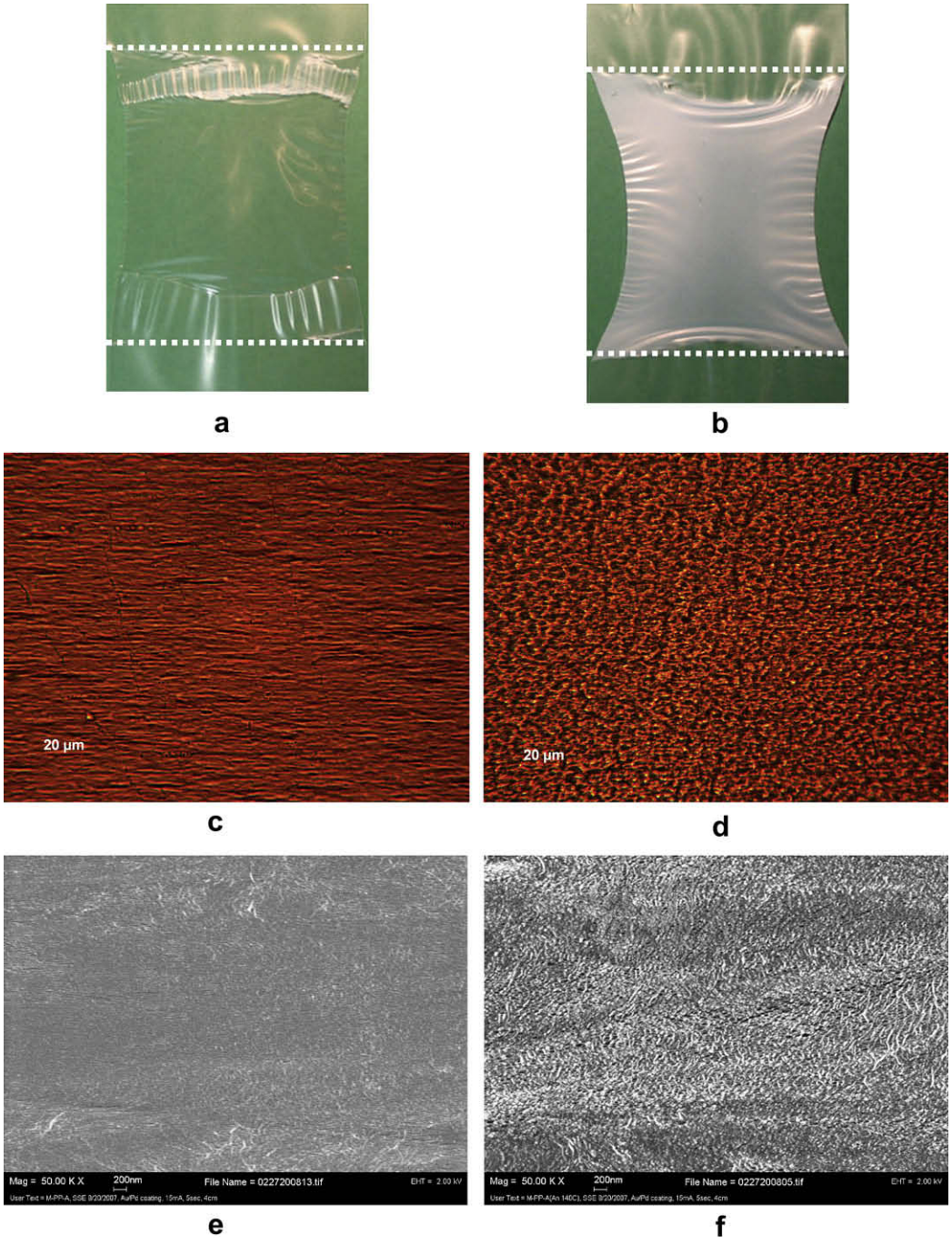

Fig. 1. Morphological examination of inter-/intra-spherulitic deformation: (a), (b) Images of M-PP and M-PP (An 140C) respectively; (c), (d) optical microscope images of M-PP and M-PP (An 140C) respectively, 400×; (e), (f) SEM images of M-PP and M-PP (An 140C) respectively, 50 000×. The stretching direction is vertical in (a) and (b), and horizontal in all other images. Stretching conditions were $E_S = 200\%$, $R_S = 12.7$ cm/min and $T_S = 25$ °C. The clamp positions are indicated by white dotted lines.

Here ρ_{cal} is the calculated density of the stretched membrane based on its fractional crystallinity (χ_c) obtained from the DSC heating scan; ρ_c is the density of the crystalline region taken as 0.946 g/cm^3; ρ_a is the density of the amorphous region taken as 0.855 g/cm^3 [11]; V_{cal} is the calculated volume of a stretched membrane of measured mass M_M and density ρ_{cal}; V_M is the measured volume of the stretched membrane with an area of 17.8 cm^2 and its measured thickness. The quantity ε can therefore be obtained from the difference of V_{cal} and V_M divided by V_{cal}.

3. Results and discussion

3.1. Effect of extrusion and annealing conditions

To produce un-oriented spherulitic precursor films, a series of extrusion conditions were examined, which included variations of extrusion temperature, extrusion rate, take-up speed and take-up temperature. It was found that the spherulitic structure could be reproduced under low-stress extrusion conditions such as high extrusion temperature, low extrusion rate, and low take-up speed. The effect of extrusion temperature was not found to be critically important for generating membranes with inter-spherulitic deformation, as long as the extrusion temperature was high enough to achieve low-stress extrusion conditions. The spherulitic characteristics of the precursor films were affected by the rate of cooling during extrusion; the temperature control on the take-up rolls also played an important role in attaining uniform precursor films. In general, a fast cooling rate produces more nucleation sites, and generates smaller spherulites [16].

On the other hand, the variation of the cooling rate also influences the crystallographic and lamellar characteristics of the spherulites [12]. This could be quite complicated in the case of PP which has four distinct crystallographic forms (α-, β-, γ-, and smectic) [17], and each of them has its own properties. The α-form is the most common crystallographic form with a unique cross-hatched lamellar morphology (R-lamellae intermeshed with T-lamellae with a branching angle of 80°). The proportion of R-lamellae and T-lamellae in the α-form is also affected by the cooling rate [18,19]. Our previous work [6] has shown that it is important to produce α-spherulites with high fraction of T-lamellae in order to promote the occurrence of inter-spherulitic deformation. The fast cooling rate which can be applied by lowering the roll temperature does promote the formation of T-lamellae. On the other hand, it may also restrain the growth of spherulites and create weaker spherulites. Because the spherulitic deformation mechanism of the precursor films is also affected by its lamellar and spherulitic characteristics, a further discussion on the influence of these characteristics will exceed the scope of this investigation. Therefore, a fixed set of extrusion conditions was chosen for producing precursor films with similar spherulitic properties.

Morphological and crystallographic characterizations of precursor films extruded under the low-stress extrusion conditions have been summarized in our previous study [6]. In brief, these extrusion conditions can produce the T-lamellae-rich α-spherulites which show a positive sign of birefringence with a first- and third-quadrant blue in Maltese cross pattern under cross-polarizing optical microscope with a first order λ-plate between polarizers [12]. The annealing process was important to promote inter-spherulitic deformation due to the strengthened lamellar structure at the high temperature. The occurrence of inter-spherulitic deformation was observed in the sample annealed at 140 °C under the investigated stretching conditions. The results of morphological characterization of the stretched membranes are shown in Fig. 1.

Upon stretching, the non-annealed stretched membrane (M-PP) (Fig. 1(a)) exhibited a typical necking and cold-drawing behavior ("M" is used to designate stretched membranes). The cold-drawn

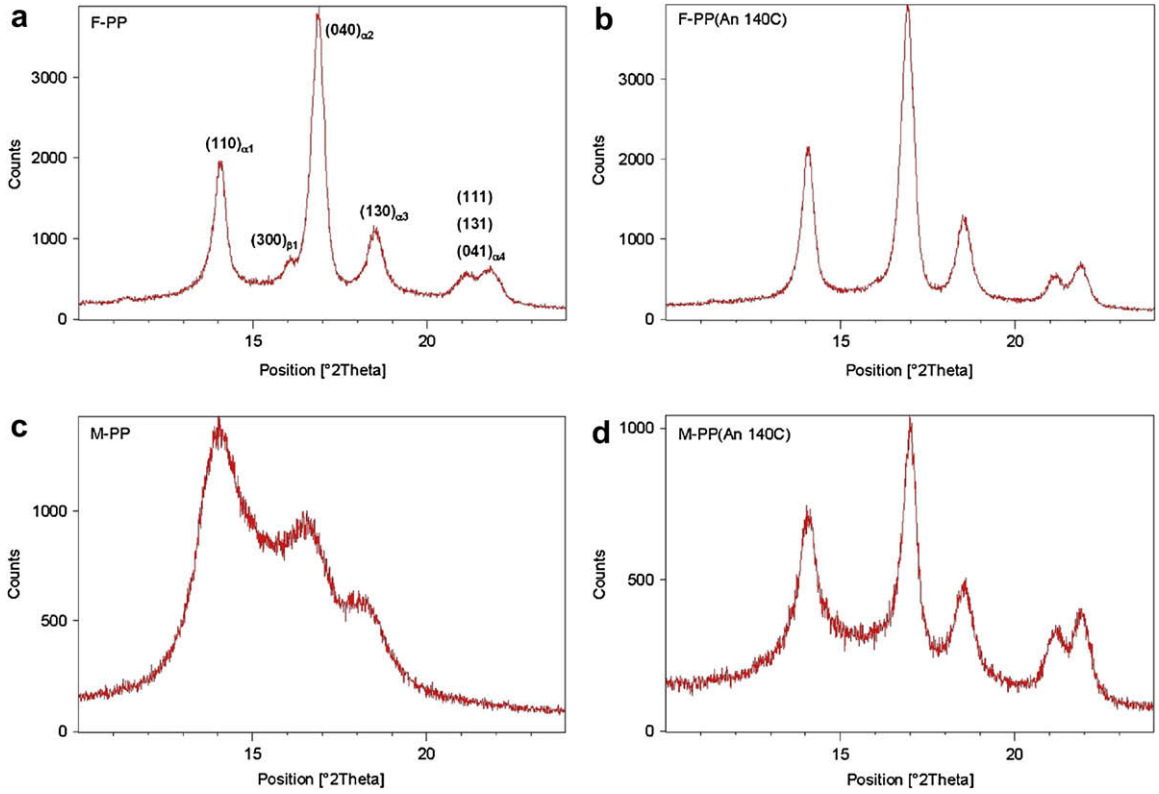

Fig. 2. Crystallographic examinations of inter-/intra-spherulitic deformation: (a), (b) WAXS spectra of F-PP and F-PP (An 140C) respectively; (c), (d) WAXS spectra of M-PP and M-PP (An 140C) respectively. Stretching conditions were $E_S = 200\%$, $R_S = 12.7$ cm/min, and $T_S = 25$ °C.

region is transparent due to the orientation of the lamellae. The border line between cold-drawn and non-deformed region can be easily distinguished by the differences in transparency. The clamp positions are indicated by white dotted lines in Fig. 1(a) and (b). The optical microscope image of the cold-drawn region of the non-annealed M-PP sample shows an elongated morphology in Fig. 1(c). The annealed M-PP (An 100C) and M-PP (An 120C) samples showed a similar appearance as the M-PP sample. However, the sample annealed at higher temperature M-PP (An 140C) shows a distinct opaque appearance in Fig. 1(b). The opaque region covered almost the entire stretched area between the clamps.

Unlike a typical cold-drawn sample, the M-PP (An 140C) sample shows a discrete morphology in the optical microscope image (Fig. 1(d)). The opaque appearance is believed to be the result of light scattering at the interface of microdomains. The SEM images of both annealed and non-annealed samples show typical cross-hatched lamellar morphology of the α-form (Fig. 1(e) and (f)). The lamellar openings (pores) are evident in the M-PP (An 140C) sample with a pore size in the range of 50–100 nm presumably due to the occurrence of inter-spherulitic deformation. However, the lamellar openings are extensively reduced in the M-PP sample as a result of catastrophic chain breaking, orienting and packing after intra-spherulitic deformation.

3.2. α-Form orientation index and its correlation to porosity

In addition to the microscopic examination on a spherulitic scale, the intra-/inter-spherulitic transition can also be detected on a lamellar scale by WAXS examination. With intra-spherulitic deformation, spherulites are deformed and elongated; therefore, lamellae are also oriented along the stretching direction. A highly oriented lamellar structure is expected in the cold-drawn region such as the transparent region in Fig. 1(a). On the contrary, spherulites are much less deformed with inter-spherulitic deformation and lamellae are capable of maintaining their isotropy within the spherulites.

The WAXS spectra of the precursor films, F-PP and F-PP (An 140C) ("F" is used to designate precursor films), are shown in Fig. 2(a) and (b). A significant amount of α-form is evident and a traceable amount of β-form (β_1: 16.1° (300)) disappeared by annealing at 140 °C [20]. The difference of intra- and inter-spherulitic deformation is represented in the WAXS spectra of the stretched membranes in Fig. 2(c) and (d).

The main crystallographic planes of the α-form can be categorized into two plane groups [21]. The plane group I includes α_1: 14.1° (110), α_2: 16.9° (040) and α_3: 18.5° (130) peaks, which are normal to the (001) plane (*c*-axis direction). The plane group II is the lumped α_4 (21.3° (111), 21.8° (131) and 21.9° (041)) peak which is inclined to the surface of the lamellae. In the one-dimensional WAXS experiment, the crystallographic planes can only be detected when they are parallel to the sample surface. Since spherulites consist of lamellae growing isotropically outward from the center of the nucleating sites, both plane groups can be detected in the undeformed spherulites. This is shown in the WAXS spectra of the spherulitic precursor films in Fig. 2(a) and (b).

The spherulites can lose crystallographic isotropy due to the orientation of lamellae following a catastrophic intra-spherulitic deformation. In a fully oriented sample, the *c*-axis of the deformed lamellae is aligned toward the stretching direction. Therefore, only the crystallographic planes perpendicular to the *c*-axis can be detected. As a result, the disappearance of plane group II would be expected. This is shown in the typical cold-drawn M-PP sample in Fig. 2(c). On the other hand, the presence of the plane group II in the M-PP (An 140C) sample in Fig. 2(d) implies a high degree of lamellar isotropy due to a less-deformed spherulite with inter-spherulitic deformation. This implies that the WAXS spectra of the stretched membranes can be used to indicate the occurrence of inter-spherulitic deformation.

Table 1
The α-form orientation index (*A*), porosity, and crystallinity of precursor films and stretched membranes.

Samples	Stretching conditions			*A*	Crystallinity (χ_c)	Porosity (ε)
	E_S (%)	R_S (cm/min)	T_S (°C)			
F-PP				0.82	0.43	–
F-PP (An 100C)				0.81	0.48	–
F-PP (An 120C)				0.80	0.49	–
F-PP (An 140C)				0.80	0.51	–
M-PP	200	12.7	25	0.98	0.42	0.06
M-PP (An 100C)	200	12.7	25	0.99	0.46	0.02
M-PP (An 120C)	200	12.7	25	0.92	0.48	0.03
M-PP (An 140C)	200	12.7	25	0.62	0.49	0.18

A quantitative characterization of the lamellar orientation using WAXS spectra was suggested by Trotignon et al. [22]. The α-form orientation index (*A*) is defined as follows:

$$A = \frac{h\alpha_1}{h\alpha_1 + h\alpha_4} \tag{4}$$

where $h\alpha_1$ and $h\alpha_1$ are the heights of the corresponding crystalline peaks taken from the amorphous background. $A = 1$ in a fully oriented sample since there will be no α_4 peak in the WAXS spectrum. According to Ref. [22], $A = 0.57$ for an isotropic sample.

A comparison of the *A* values of the precursor films and the corresponding stretched membranes is shown in Table 1 for a given set of stretching conditions ($R_S = 12.7$ cm/min, $E_S = 200\%$, and $T_S = 25$ °C). The *A* value for the non-annealed F-PP sample was 0.82, and slightly decreased with increasing annealing temperature ($A = 0.81$ of the F-PP (An 100C) sample and 0.80 for the F-PP (An 140C) sample). The somehow high orientation index of the precursor films indicates pre-orientation of chains induced by the extrusion process, and rearrangement of these chains at the high annealing temperature. The *A* value of the non-annealed stretched membrane (M-PP) was 0.98 which indicates a nearly fully oriented sample and is consistent with the morphological observations in Fig. 1. Annealing temperatures of 100 °C and 120 °C did not promote the occurrence of inter-spherulitic deformation at the investigated stretching conditions since $A = 0.99$ for the annealed stretched membrane M-PP (An 100C), and 0.92 for the M-PP (An 120C) sample. However, a higher annealing temperature of 140 °C did trigger inter-spherulitic deformation which is shown in the M-PP (An 140C) sample with an *A* value of 0.62. This represents a high degree of isotropy of the lamellar structure in the film even when it

Table 2
The α-form orientation index (*A*), porosity, and crystallinity of membranes stretched at different stretching ratios.

Samples	Stretching conditions			*A*	Crystallinity (χ_c)	Porosity (ε)
	E_S (%)	R_S (cm/min)	T_S (°C)			
M-PP	100	12.7	25	0.98	0.42	0.04
M-PP	200	12.7	25	0.98	0.42	0.06
M-PP	300	12.7	25	0.98	0.41	0.02
M-PP	400	12.7	25	0.99	0.41	0.03
M-PP	500	12.7	25	1.00	0.42	0.02
M-PP	600	12.7	25	1.00	0.41	0.02
M-PP (An 140C)	100	12.7	25	0.58	0.50	0.22
M-PP (An 140C)	200	12.7	25	0.62	0.49	0.18
M-PP (An 140C)	300	12.7	25	0.74	0.49	0.11
M-PP (An 140C)	400	12.7	25	0.76	0.48	0.09
M-PP (An 140C)	500	12.7	25	0.87	0.47	0.08
M-PP (An 140C)	600	12.7	25	0.91	0.47	0.06

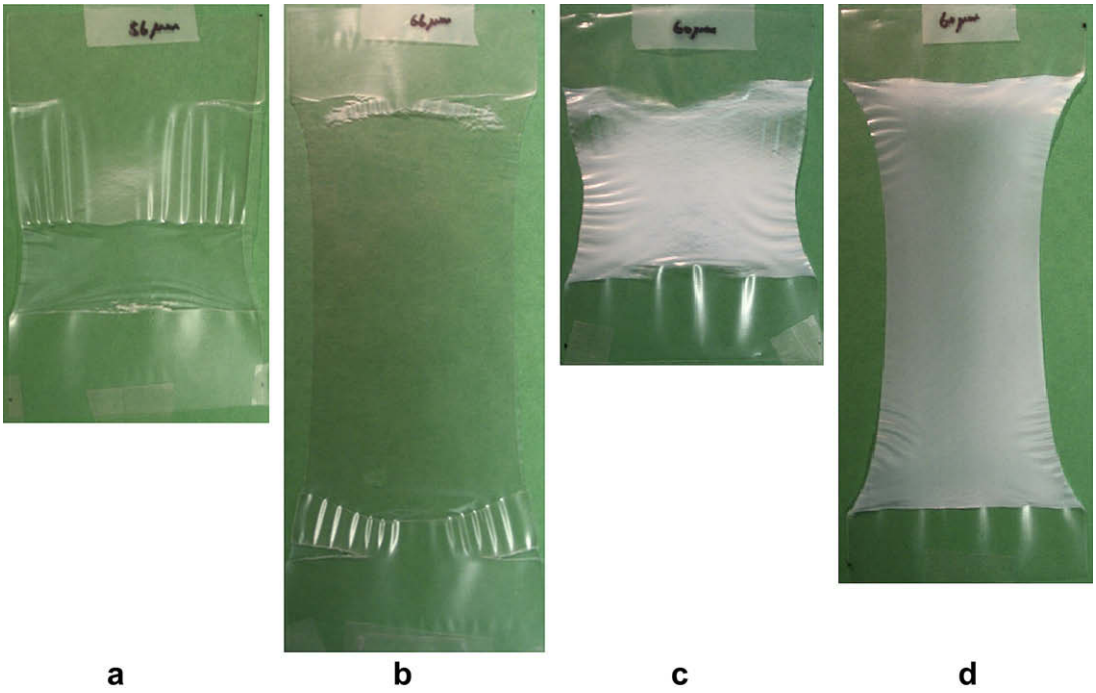

Fig. 3. Images of membranes stretched at different E_S: (a) M-PP ($E_S = 100\%$); (b) M-PP ($E_S = 400\%$); (c) M-PP (An 140C) ($E_S = 100\%$); (d) M-PP (An 140C) ($E_S = 400\%$). Stretching conditions were $R_S = 12.7$ cm/min and $T_S = 25$ °C.

was stretched up to 200% of its original length. This value is lower than that of its precursor film F-PP (An 140C). This may indicate that the pre-oriented lamellae within the spherulites were able to rebound and be restored to a more isotropic state due to the loosened spherulitic boundary during inter-spherulitic deformation.

The results of crystallinity and porosity of the stretched membranes are also summarized in Table 1. Annealing at 140 °C results in the highest crystallinity for both unstretched and stretched samples. The porosity of the stretched samples, M-PP, M-PP (An 100C), and M-PP (An 120C) samples is low, about 0.02–0.06. However, a much higher porosity (0.18) is observed in the M-PP (An 140C) sample. The low porosity of the samples with a high α-form orientation index represents the result of chain orientation and packing in these stretched membranes. On the other hand, the higher porosity of the sample with a low α-form orientation index indicates that the porous structure (lamellar openings) was preserved by the less-deformed spherulites.

3.3. Effect of extension ratio

The effect of extension ratio on the intra-spherulitic and inter-spherulitic deformations was investigated by stretching the precursor films F-PP and F-PP (An 140C) at extension ratios ranging from 100% to 600% at $R_S = 12.7$ cm/min and $T_S = 25$ °C. Results are shown in Table 2. Some noteworthy images of the stretched membranes are shown in Fig. 3. A typical cold-drawn behavior was observed in the non-annealed stretched membranes showing transparent cold-drawn and non-cold-drawn regions. The proportion of the cold-drawn region increases and that of the non-deformed region decreases with increasing extension ratio as shown

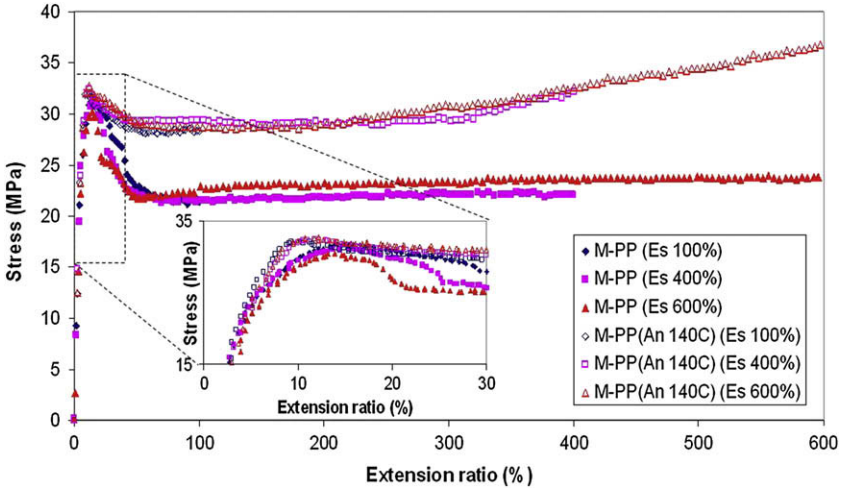

Fig. 4. Stress–strain curves of membranes stretched at different E_S. Stretching conditions were $R_S = 12.7$ cm/min and T_S 25 = °C.

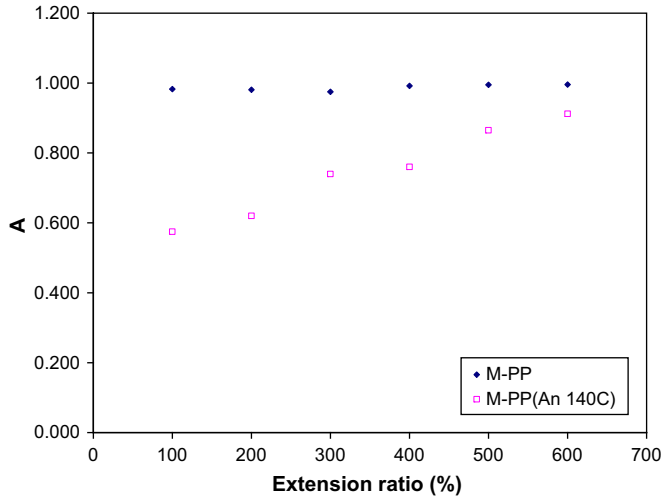

Fig. 5. α-Form orientation index (A) of membranes stretched at different E_S. Stretching conditions were R_S 12.7 = cm/min and $T_S = 25$ °C.

in Fig. 3(a) and (b). For the annealed stretched membranes, an opaque appearance within the stretched region is observed (Fig. 3(c) and (d)). The width in the middle of these samples decreased with increasing extension ratio.

Stress–strain curves of membranes stretched at different E_S are shown in Fig. 4. All non-annealed and annealed samples exhibited similar ductile behavior, and there was no significant difference in their initial tensile modulus. The annealed samples showed slightly higher yield stress than the non-annealed samples, and a tougher behavior with a larger area under the curves. A strain-hardening behavior was observed in the annealed samples but not in the non-annealed samples within the investigated range. The annealed samples showed a more brittle behavior with a lower yield strain (~11%) than the non-annealed samples (~15%) (Fig. 4, inset). This may be related to the presence of different sites of yielding corresponding to inter- and intra-spherulitic deformations, respectively [23]. For example, the yielding site for the inter-spherulitic deformation of the annealed samples might be initiated at the spherulitic boundaries due to a more rigid spherulitic structure, and as a result a lower value of yield strain is obtained.

Table 3
The α-form orientation index (A), porosity and crystallinity of membranes stretched at different stretching rates (stretching temperature 25 °C).

Samples	Stretching conditions			A	Crystallinity (χ_c)	Porosity (ε)
	E_S (%)	R_S (cm/min)	T_S (°C)			
M-PP	200	50.8	25	0.99	0.41	0.02
M-PP	200	25.4	25	0.99	0.42	0.03
M-PP	200	12.7	25	0.98	0.42	0.06
M-PP	200	2.54	25	0.99	N/M[a]	N/M
M-PP	200	1.27	25	0.98	N/M	N/M
M-PP	200	0.25	25	0.98	N/M	N/M
M-PP (An 140C)	200	50.8	25	0.98	0.47	0.03
M-PP (An 140C)	200	25.4	25	0.69	0.48	0.04
M-PP (An 140C)	200	12.7	25	0.62	0.49	0.18
M-PP (An 140C)	200	2.54	25	0.63	N/M	N/M
M-PP (An 140C)	200	1.27	25	0.67	N/M	N/M
M-PP (An 140C)	200	0.25	25	0.72	N/M	N/M

[a] N/M is not measured due to uneven surface of the sample at very slow stretching rate.

The plot of the α-form orientation index versus extension ratio is shown in Fig. 5. The A values of the non-annealed samples were about 1. As mentioned in previous sections, the cold-drawing behavior represents lamellae breaking and alignment along the stretching direction. The higher extension ratio simply created more cold-drawn regions, and the lamellae in these regions remained highly oriented. By contrast, the A values of the annealed samples increased with increasing extension ratio. The A value of the annealed stretched sample at 100% extension ratio was only 0.58; this low value suggests the recovery of pre-oriented spherulites in the earlier stage of inter-spherulitic deformation. Note that the annealed sample could be stretched up to 600% of its original length without fracture. This indicates that the residual lamellae at the separated spherulitic boundary were strong enough to prevent sample rupture. The spherulites of inter-spherulitic deformation started to orient with increasing extension ratio which implied the occurrence of intra-spherulitic deformation at the late stage of stretching. As a result, the A value of the annealed stretched sample at 600% extension ratio was 0.91 which was close to that of the fully oriented sample.

The porosity of samples produced at different extension ratios is shown in Fig. 6. The porosity of non-annealed samples was about 0.02–0.06, and did not show a significant change with extension ratio. Since increasing the extension ratio of the non-annealed

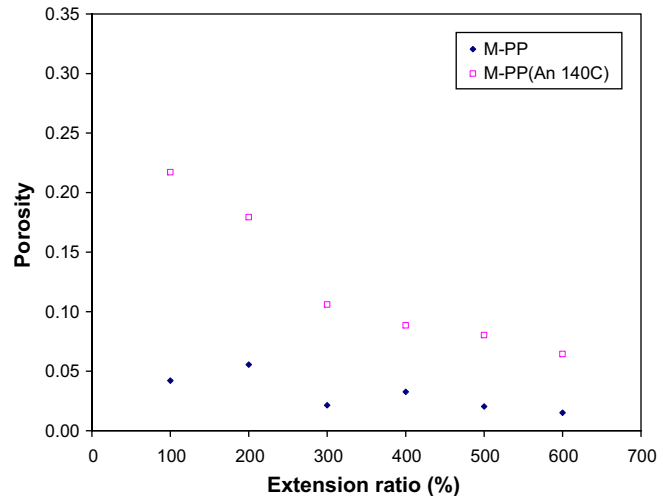

Fig. 6. Porosity of membranes stretched at different E_S. Stretching conditions were $R_S = 12.7$ cm/min and $T_S = 25$ °C.

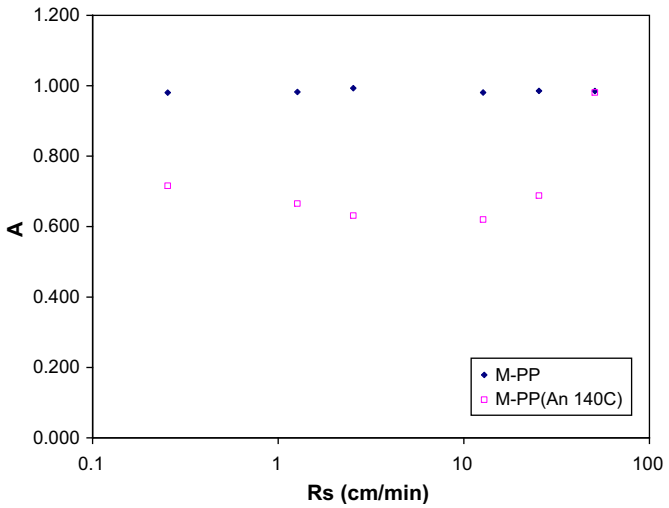

Fig. 7. α-Form orientation index (A) of membranes stretched at different R_S. Stretching conditions were $E_S = 200\%$ and $T_S = 25$ °C.

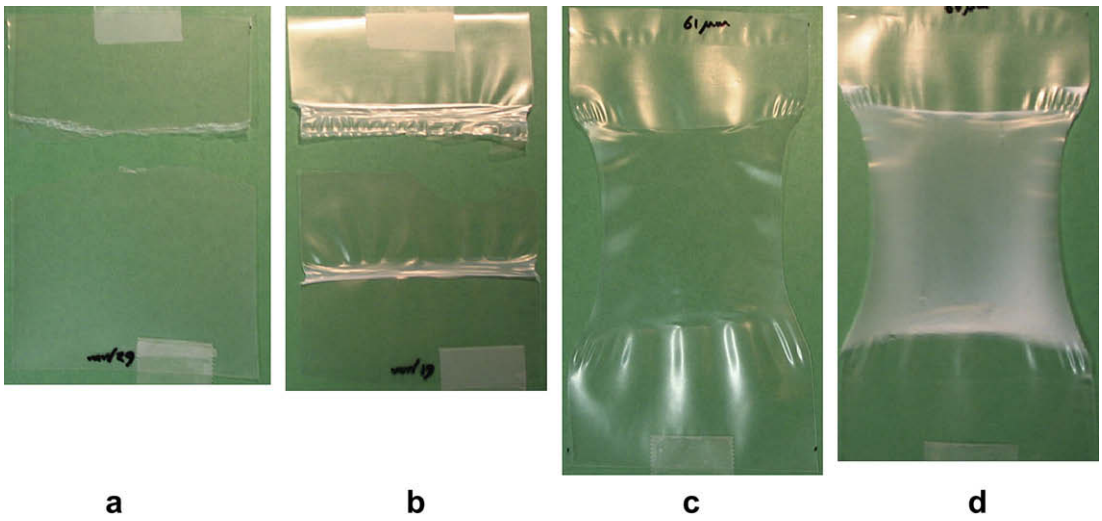

Fig. 8. Images of membranes stretched at different T_S: (a), (b) images of M-PP and M-PP (An 140C) at $T_S = -20$ °C respectively; (c), (d) images of M-PP and M-PP (An 140C) at $T_S = 70$ °C respectively. Stretching conditions were $E_S = 200\%$ and $R_S = 12.7$ cm/min.

samples only enlarged the cold-drawn region which was already fully oriented, a similar porosity is expected. The porosity of the annealed samples decreased with increasing extension ratio, which is consistent with the opposite trend for the α-form orientation index (Fig. 5). Thus, the highest porosity attained so far was about 0.18 at an extension ratio of 100%. However, a low extension ratio is not necessarily a good strategy to improve porosity, since the unevenly deformed region at a low extension ratio (Fig. 3(c)) could limit the membrane area available for permeation.

As discussed earlier, the porous structure is generated by the separation of lamellae, and a similar pore size is observed throughout the entire SEM micrographs in the lamellar morphology. The permeability of the membranes should be proportional to their porosity, as a result of their similar pore characteristics.

3.4. Effect of stretching rate

The effect of stretching rate on intra- and inter-spherulitic deformations was investigated by stretching the precursor films F-PP and F-PP (An 140C) at a stretching rate ranging from 0.25 cm/min to 50.8 cm/min with $E_S = 200\%$ and $T_S = 25$ °C. Results are shown in Table 3. The effect of stretching rate on the α-form orientation index is shown in Fig. 7. The non-annealed samples showed high A values within the investigated range. For the annealed samples, intra-spherulitic deformation was only evident at the highest stretching rate ($R_S = 50.8$ cm/min). An apparent inter-spherulitic deformation with low A values was found at other stretching rates.

In general, polymers show ductile behavior at low stretching rates and brittle behavior at high stretching rates [7,24]. In this study, even though all samples showed a ductile behavior with no sign of fracture, differences in the apparently similar ductile behaviors can be distinguished from their microstructures. The ductile behavior of the non-annealed samples is the result of lamellae breaking and orientation inside the spherulites. However, the ductile behavior shown in the samples with inter-spherulitic deformation may be due to the presence of tough residual lamellae at the separated spherulitic boundary. Inter-spherulitic deformation should be more pronounced at a low stretching rate, since the generated stress could be transmitted to a weak site, such as a spherulite boundary. On the other hand, intra-spherulitic deformation would be more favored to occur at a high stretching rate.

The porosity of the samples produced at different stretching rates (Table 3) confirms the results from the WAXS analysis. The porosity of the annealed samples increased with decreasing stretching rate. A low porosity (0.03) of the annealed sample at the highest stretching rate ($R_S = 50.8$ cm/min) is attributed to the intra-spherulitic deformation. Since the surface of the stretched membranes became uneven at stretching rates lower than 2.54 cm/min, porosity at low stretching rates could not be measured. Thus, there is an apparent limitation in using low

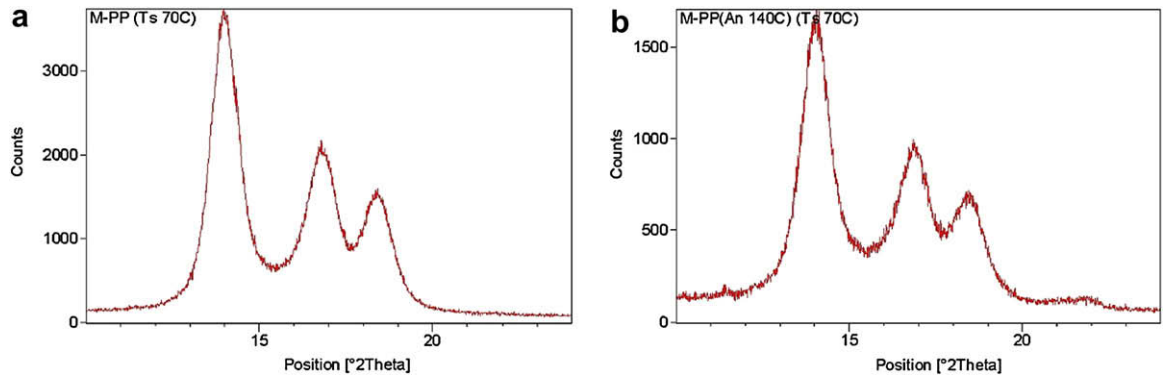

Fig. 9. Crystallographic examinations of inter-/intra-spherulitic deformation: (a) M-PP; (b) M-PP (An 140C). Stretching conditions were $E_S = 200\%$, $R_S = 12.7$ cm/min, and $T_S = 70$ °C.

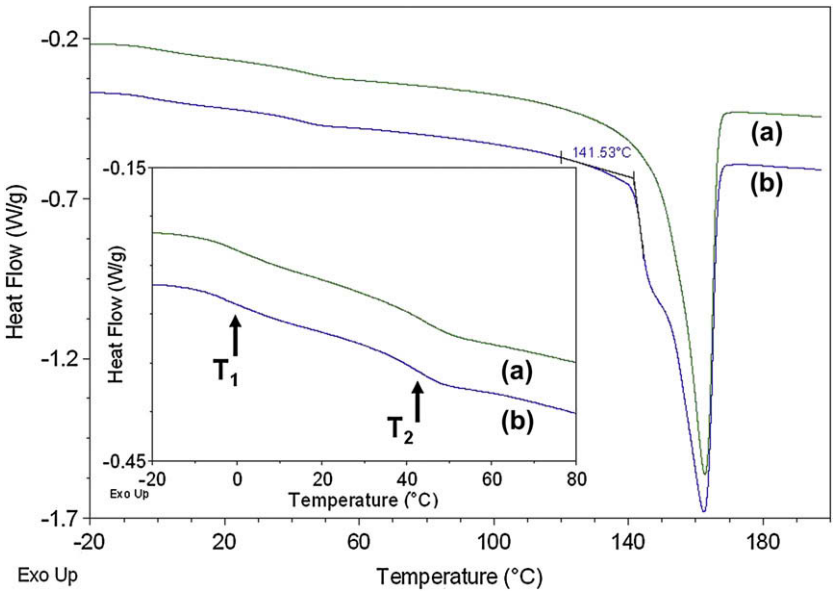

Fig. 10. DSC heating scan of precursor films (first heating): (a) F-PP and (b) F-PP (An 140C).

stretching rates to promote inter-spherulitic deformation. The localized effects on specific weak sites, such as the boundaries around larger spherulites that also endure higher stresses, become predominant at much lower stretching rates resulting in an unevenly deformed structure.

3.5. Effect of stretching temperature

The effect of stretching temperature on intra- and inter-spherulitic deformations was investigated by stretching the precursor films F-PP and F-PP (An 140C) at stretching temperatures of −20 °C, 25 °C, and 70 °C with $R_S = 12.7$ cm/min and $E_S = 200\%$. A low stretching temperature of −20 °C was chosen to observe the mechanical response of the precursor films below the T_g of PP (about −5 °C). Brittle fracture images of samples stretched at 12.5 cm/min are shown in Fig. 8(a) and (b).

For a stretching temperature higher than the T_g of PP, a cold-drawn appearance is expected, as shown in Fig. 1(a) and (b). The images of samples stretched at 70 °C are shown in Fig. 8(c) and (d). Interestingly, the appearance of these films did not meet our expectations. The non-annealed sample (Fig. 8(c)) did not have the same appearance as the typical cold-drawn pattern (Fig. 1(a)), even though it was still transparent. In fact, it had a narrower width in the middle of the deformed region which resembled the appearance of the annealed sample (Fig. 1(b)). Furthermore, the occurrence of inter-spherulitic deformation should be more significant in the annealed sample due to a more flexible amorphous phase at higher stretching temperature. As a result, a more opaque appearance would be expected in the annealed sample. However, a less opaque appearance is shown in Fig. 8(d).

The WAXS spectra of the samples stretched at 70 °C are shown in Fig. 9(a) and (b), where the diminishing α_4 peak indicates the

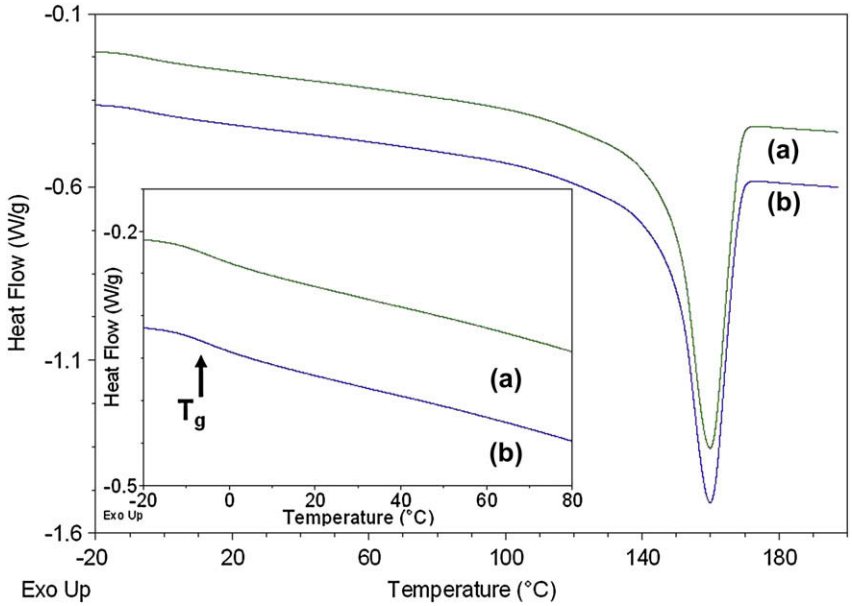

Fig. 11. DSC heating scan of precursor films (second heating): (a) F-PP and (b) F-PP (An 140C).

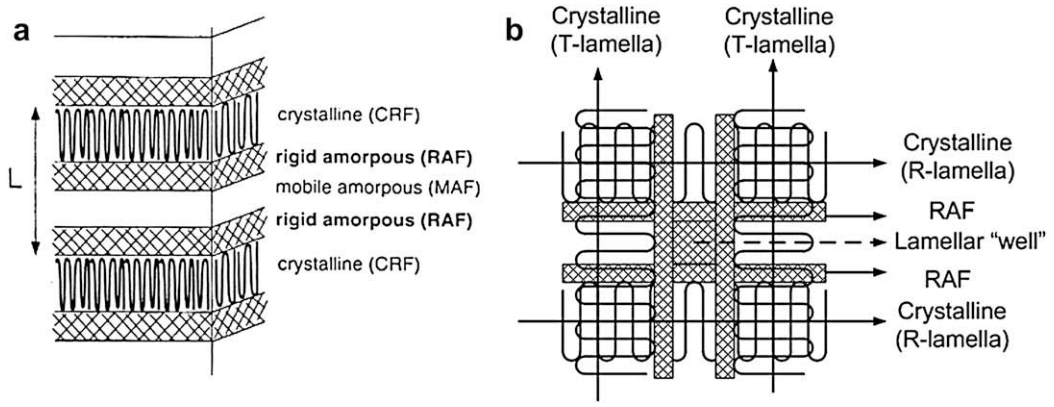

Fig. 12. Schematic of RAF: (a) in conventional semicrystalline polymers [30]; (b) in T-lamellae-rich, α-form polypropylene of this work.

occurrence of intra-spherulitic deformation in both samples. Another noteworthy observation is the well-divided peaks in the WAXS spectra, which implies fewer broken lamellae. These unexpected observations of the effect of stretching temperature suggest the presence of an unidentified transition between 25 °C and 70 °C. In order to elucidate this transition, a detailed thermal analysis was conducted on the precursor films.

The results of the DSC heating scans of the F-PP and F-PP (An 140C) samples are shown in Fig. 10. For both samples, a clear melting peak at 162 °C is evident, which represents the melting temperature of the major lamellae. For the F-PP (An 140C) sample, a shoulder with an onset temperature of 141.5 °C is observed which represents the thickening of lamellae by the annealing process; the onset temperature is corresponding to the annealing temperature [25]. Similar features are also found in the F-PP (An 100C) and F-PP (An 120C) samples [6].

A distinct feature was found by analyzing the glass transition temperature of these samples. Actually, in both samples (Fig. 10(a), inset), there were two endothermic discontinuities T_1 and T_2 at 0 °C and 40 °C respectively with the first resembling the glass transition temperature of PP. These two discontinuities were found in all precursor films (annealed or non-annealed). After keeping the samples at 230 °C for 10 min to erase their thermal history, cooling down to −50 °C and heating for a second time, a single discontinuity is shown at −5 °C (Fig. 11, inset), and a melting peak at 160 °C (Fig. 11). Thus, it is reasonable to assume that the T_1 of the first scan represented the conventional T_g of polypropylene, and that T_2 is not related to melting of the crystalline domains since it would have disappeared by annealing at high temperatures (140 °C).

The presence of a second relaxation (above T_g) of PP has been shown by DMTA analysis [26–28]. The unusual relaxation signal around 50–80 °C is believed to result from crystal–crystal slip in polypropylene. Similar peaks were also observed in a limited number of DMTA conducted in the present work. However, since the frequency-dependent behavior of DMTA data requires considerable analysis, only the DSC results are included in this study. It is known that DMTA is more sensitive than DSC in recognizing relaxation processes such as glass transition. This might be the reason for the lack of data by DSC analysis on this subject. So far, a similar observation by DSC analysis has only been shown by Hedesiu et al. (Fig. 5(a) in Ref. [29]) who did not offer a detailed explanation. A possible explanation for the apparent endothermic discontinuity observed in our DSC analysis could originate from the concept of rigid-amorphous fraction (RAF).

The existence of RAF in semicrystalline polymers has been studied for two decades [30,31]. Since polymer chains are continuous across the amorphous phase and crystalline phases, RAF is an interfacial amorphous layer between these phases, whose chain mobility is restricted due to the locking segments at the crystalline phase (lamellae) as shown in Fig. 12(a). As a consequence, the existence of RAF results in an increase in glass transition temperature or its broadening. In the α-form PP, the intermeshed morphology of R-lamellae and T-lamellae might increase the proportion of RAF. The resultant confinement by the lamellar structure could be emphasized by the amorphous region surrounded by R-lamellae and T-lamellae that we call lamellar "wells" as shown in Fig. 12(b). This hypothesis also implies that the potential locations of RAF are those lamellar "wells" inside the spherulites. There is little RAF at the spherulitic boundary due to the more mobile entrant chains from the non-stacked impinged lamellae [32]. This could explain the presence of the high amount of the amorphous phase corresponding to the second endothermic discontinuity (T_2), which is comparable to the first endothermic discontinuity (T_1). The high proportion of T-lamellae in the spherulites of the precursor film may be related to fast cooling during the extrusion process.

The effect of stretching temperature on the deformation mechanism of the PP precursor films with significant amount of RAF can then be explained as follows: (1) As the stretching temperature is below T_g, the samples fracture in a brittle manner due to the frozen amorphous phase. (2) As the stretching temperature is between T_g and T_2, the spherulite boundary is flexible but the lamellar "wells" are still rigid due to the high proportion of RAF trapped by T-lamellae and R-lamellae. In the case of weak lamellae (non-annealed sample),

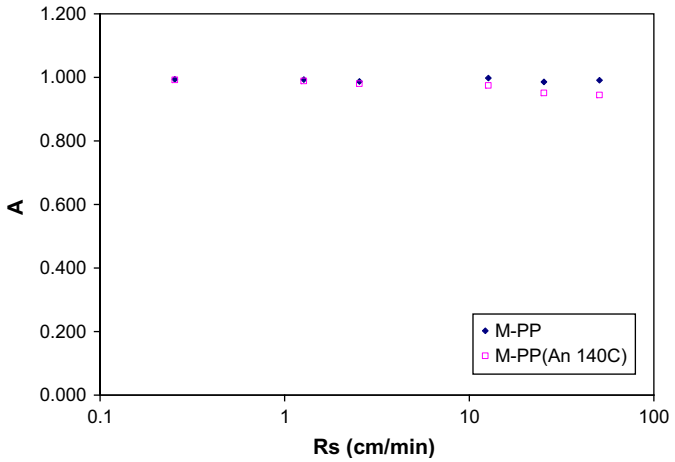

Fig. 13. α-Form orientation index (A) of membranes stretched at different R_S. Stretching conditions were $E_S = 200\%$ and $T_S = 70$ °C.

Table 4
The α-form orientation index (A), porosity, and crystallinity of membranes stretched at different stretching rates (stretching temperature 70 °C).

Samples	Stretching conditions			A	Crystallinity (χ_c)	Porosity (ε)
	E_S (%)	R_S (cm/min)	T_S (°C)			
M-PP	200	50.8	70	0.99	0.41	0.03
M-PP	200	25.4	70	0.99	0.42	0.01
M-PP	200	12.7	70	1.00	0.41	0.02
M-PP	200	2.54	70	1.00	N/M[a]	N/M
M-PP	200	1.27	70	0.99	N/M	N/M
M-PP	200	0.25	70	0.99	N/M	N/M
M-PP(An 140C)	200	50.8	70	0.95	0.49	0.07
M-PP(An 140C)	200	25.4	70	0.95	0.50	0.04
M-PP(An 140C)	200	12.7	70	0.98	0.50	0.05
M-PP(An 140C)	200	2.54	70	0.98	N/M	N/M
M-PP(An 140C)	200	1.27	70	0.99	N/M	N/M
M-PP(An 140C)	200	0.25	70	0.99	N/M	N/M

[a] N/M is not measured due to uneven surface of the sample at very slow stretching rate.

the lamellae around the lamellar "wells" are broken and aligned toward the stretching direction. The RAF alone is not strong enough to maintain this morphology. As a result, a typical cold-drawn appearance is shown as in Fig. 1(a). However, in the case of strong lamellae (annealed sample), the combined strength of lamellae and RAF is sufficiently high to hold up the lamellar "wells" and the spherulitic morphology; as a result, inter-spherulitic deformation is shown as in Fig. 1(b). (3) As the stretching temperature is higher than T_2, the entire amorphous region is flexible, and the effect of RAF is minimized. The lamellar "wells" can no longer provide the strength to sustain the morphology. The lamellae could break down or slip from the lamellar knots, which would depend on the strength of the lamellae. As a result, the annealed lamellae can still be oriented without catastrophic cold-drawn deformation (Fig. 8(c) and (d)).

Fig. 13 shows the effect of the stretching rate on the α-form orientation index at a stretching temperature of 70 °C. All non-annealed and annealed samples appear highly oriented. Compared to Fig. 7 where annealed samples showed low orientation at low stretching rates at 25 °C, the results support the proposed role of RAF in preventing intra-spherulitic deformation. The combination of RAF with enhanced strength lamellae seems to form a criterion for initiating inter-spherulitic deformation. The results of the α-form orientation index, crystallinity and porosity of samples stretched at 70 °C are summarized in Table 4.

4. Concluding remarks

The processing boundaries for utilizing intra-/inter-spherulitic deformation to create microporous membranes by lamellar separation have been delineated. The investigated conditions included: annealing temperature, extension ratio, stretching rate, and stretching temperature. A fixed set of extrusion conditions was chosen for producing precursor films with similar spherulitic properties. A typical cold-drawn behavior (catastrophic intra-spherulitic deformation) was shown in the non-annealed sample with a transparent appearance and an elongated morphology. Inter-spherulitic deformation was found with a distinct opaque appearance with a discrete morphology in the sample annealed at 140 °C. The lamellar openings (pores) were evident in the M-PP (An 140C) sample with a pore size in the range of 50–100 nm due to the occurrence of inter-spherulitic deformation. The microscopic evidences representing the occurrence of intra-/inter-spherulitic transition in the spherulitic scale can also be detected in the lamellar scale by WAXS examination. A highly oriented sample showed a high value of α-form orientation index and a spherulitic sample with a high degree of lamellar isotropy showed a low value of α-form orientation index. The porosity measurements of the stretched membranes showed a consistent correlation with their α-form orientation index.

The increasing extension ratio did not change the microstructure of the deformed region in the intra-spherulitic deformation sample, where the proportion of the cold-drawn region increased and the non-deformed region decreased with increasing extension ratio. However, the microstructure of the inter-spherulitic deformation sample can be oriented with increasing extension ratio. In this study, the residual lamellae at separated spherulitic boundaries were strong enough to prevent sample rupture. Inter-spherulitic deformation became obvious at slow stretching rate, since the stress generated by stretching would have time to transmit to the weak sites, such as spherulite boundaries. On the other hand, intra-spherulitic deformation was more favored to occur at a fast stretching rate.

At high stretching temperatures, an expected typical cold-drawn appearance did not show in the non-annealed sample, and a less opaque appearance was found in the annealed sample. These unexpected behaviors are believed to be influenced by the rigid-amorphous fraction (RAF) trapped inside the cross-hatched lamellar morphology of α-PP. The DSC thermal analysis on the precursor films showed two distinct endothermic discontinuities; one was at 0 °C (T_1) and the other was at 40 °C (T_2). T_1 is believed to be the conventional T_g of polypropylene, and T_2 represents the significant amount of RAF trapped within "lamellar wells" where the amorphous phase is surrounded by R-lamellae and T-lamellae. The effect of RAF is minimized as stretching temperature higher than T_2, and the amorphous phase in the "lamellar wells" cannot provide the sufficient strength to sustain the lamellar morphology. The lamellae could break down or slip from the lamellar knots, and the annealed lamellae can still be oriented without catastrophic cold-drawn deformation.

Acknowledgements

This research was financially supported by National Science Foundation under Grant DMI-0327968. The authors are very grateful to Dr. Kun Sup Hyun of the Polymer Processing Institute (PPI) for facilitating the materials acquisition and to Dr. Victor Tan (PPI) for assistance with the membrane fabrication and characterization.

References

[1] Arora P, Zhang Z. Chem Rev 2004;104:4419–62.
[2] Sprague BS. J Macromol Sci Phys 1973;B8(1–2):157–87.
[3] Chen RT, Saw CK, Jamieson MG, Aversa TR, Callahan RW. J Appl Polym Sci 1994;53:471–83.
[4] Tadmor Z, Gogos CG. Principles of polymer processing. New York: John Wiley & Sons; 1979 [chapter 3].
[5] Zhang SS. J Power Sources 2007;164:351–64.
[6] Lin KY, Xanthos M, Sirkar KK. J Membr Sci 2009;330:267–78.
[7] Schultz JM. Polym Eng Sci 1985;24:770–85.
[8] Way JY, Atkinson JR. J Mater Sci 1971;6:102–9.
[9] Way JY, Atkinson JR, Nutting J. J Mater Sci 1974;9:293–9.
[10] Perterlin A. J Mater Sci 1971;6:490–508.
[11] Pasquini N. Polypropylene handbook. 2nd ed. Munich: Hanser Gardner Publications, Inc; 2005 [chapter 3].
[12] Norton DR, Keller A. Polymer 1985;26:704–16.
[13] Lotz B, Wittmann JC. J Polym Sci Part B Polym Phys 1986;24:1541–58.
[14] Aboulfaraj M, G'Sell C, Ulrich B, Dahoun A. Polymer 1995;36:731–42.
[15] Bowen PB, Young RJ. J Mater Sci 1974;9:2034–51.
[16] Fillon B, Wittmann JC, Lotz B, Thierry A. J Polym Sci Part B Polym Phys 1993;31:1383–93.
[17] Bruckner S, Meille SV, Petraccone V, Pirozzi B. Prog Polym Sci 1991;16:361–404.
[18] Wu CM, Chen M, Karger-Kocsis J. Polymer 2001;42:199–208.
[19] Varga J. J Mater Sci 1992;27:2557–79.
[20] Li JX, Cheung WL. Polymer 1998;39:6935–40.
[21] Samios D, Tokumoto S, Denardin ELG. Macromol Symp 2005;229:179–87.
[22] Trotignon JP, Lebrun JL, Verdu J. Plast Rubber Process Appl 1982;2:247–51.
[23] Jang BZ, Uhlmann DR, Vander Sande JB. Polym Eng Sci 1985;2(25):98–104.

[24] Dijkstra PTS, Van Dijk DJ, Huetink J. Polym Eng Sci 2002;42:152–60.
[25] Poussin L, Bertin YA, Parisot J, Brassy C. Polymer 1998;39:4261–5.
[26] Boyer RF. J Macromol Sci Part B Phys 1973;B8(3–4):503–37.
[27] Boyd RH. Polymer 1985;26:323.
[28] Botev M, Neffati R, Rault J. Polymer 1999;40:5227–32.
[29] Hedesiu C, Demco DE, Kleppinger R, Vanden Poel G, Gijsbers W, Blumich B, et al. Macromolecules 2007;40:3977–89.
[30] Suzuki H, Grebowicz J, Wunderlich B. Br Polym J 1985;17(1):1–3.
[31] Androsch R, Wunderlich B. Polymer 2005;46:12556–66.
[32] Drozdov AD, Christiansen JdeC. Comput Mater Sci 2003;27:403–22.